



MIT Open Access Articles

Weather radar network benefit model for flash flood casualty reduction

The MIT Faculty has made this article openly available. **Please share** how this access benefits you. Your story matters.

Citation	Cho, John Y.N. and James M. Kurdzo, "Weather radar network benefit model for flash flood casualty reduction." <i>Journal of applied meteorology and climatology</i> 59, 4 (March 2020): p. 589-604 doi 10.1175/JAMC-D-19-0176.1 ©2020 Author(s)
As Published	10.1175/JAMC-D-19-0176.1
Publisher	American Meteorological Society
Version	Author's final manuscript
Citable link	https://hdl.handle.net/1721.1/124855
Terms of Use	Creative Commons Attribution-Noncommercial-Share Alike
Detailed Terms	http://creativecommons.org/licenses/by-nc-sa/4.0/

1 Weather Radar Network Benefit Model for Flash Flood Casualty Reduction*



2
3
4 John Y. N. Cho and James M. Kurdzo

5
6 Lincoln Laboratory, Massachusetts Institute of Technology, Lexington, Massachusetts

7
8
9
10
11
12 Corresponding Author:

13 John Y. N. Cho

14 M.I.T. Lincoln Laboratory

15 244 Wood St., S1-639

16 Lexington, MA 02421-6426

17 E-mail: jync@ll.mit.edu

18
19
20 Submitted to the *Journal of Applied Meteorology and Climatology*: 15 July 2019

21 Revised: 12 February 2020

22
23 *DISTRIBUTION STATEMENT A. Approved for public release: distribution unlimited. This material is based upon work supported
24 by the National Oceanic and Atmospheric Administration under Air Force Contract No. FA8702-15-D-0001. Any opinions, findings,
25 conclusions, or recommendations expressed in this material are those of the authors and do not necessarily reflect the views of the
26 National Oceanic and Atmospheric Administration.
27

Early Online Release: This preliminary version has been accepted for publication in *Journal of Applied Meteorology and Climatology*, may be fully cited, and has been assigned DOI 10.1175/JAMC-D-19-0176.1. The final typeset copyedited article will replace the EOR at the above DOI when it is published.

28 ABSTRACT
29

30 A monetized flash flood casualty reduction benefit model is constructed for
31 application to meteorological radar networks. Geospatial regression analyses show that
32 better radar coverage of the causative rainfall improves flash flood warning performance.
33 Enhanced flash flood warning performance is shown to decrease casualty rates.
34 Consequently, these two effects in combination allow a model to be formed that links radar
35 coverage to flash flood casualty rates. When this model is applied to the present-day
36 contiguous U.S. weather radar network, results yield a flash-flood-based benefit of \$316
37 million (M) yr⁻¹. The remaining benefit pools are more modest (\$13M yr⁻¹ for coverage
38 improvement and \$69M yr⁻¹ maximum for all areas of radar quantitative precipitation
39 estimation improvements), indicative of the existing weather radar network's effectiveness
40 in supporting the flash flood warning decision process.

41

42 **1. Introduction**

43 Weather radars are generally acknowledged to be a valuable asset to society (e.g.,
44 Saunders et al. 2018). They provide observational data that improve weather forecasts and
45 present essential situational awareness to many users. Radars, however, are expensive to
46 acquire, operate, and maintain. In planning for future sensor networks, monetization of
47 their benefits is needed to assess the trade-off between more expensive options (higher
48 performance and/or coverage) and benefits (people's lives and time saved).

49 Although meteorological radar observations help improve weather forecast model
50 performance through data assimilation (e.g., Stensrud et al. 2009), their most direct impacts
51 are made through the detailed and continuously updated depiction of precipitating weather
52 for real-time decision making. Sometimes these decisions are life or death matters. In the
53 last thirty years (1989-2018), the top three weather-related fatality causes in the U.S. were
54 excessive heat, floods, and tornadoes (NOAA 2019). The National Weather Service (NWS)
55 issues warnings for these hazards, and weather radar data plays an absolutely crucial role
56 for the latter two (Polger et al. 1994). Thus, we focused on tornadoes and floods in
57 quantifying the benefits that meteorological radars provide to society. A benefit model for
58 tornadoes was published previously (Cho and Kurdzo 2019a; Cho and Kurdzo 2019b;
59 collectively, CK19 hereafter). In this paper, we move on to a benefit model for heavy-rain-
60 induced flash floods.

61 For this study, we hypothesized that better weather radar coverage improves flash
62 flood warning performance, which, in turn, reduces casualties. The second half of this
63 causality chain is intuitive. Flash flood warnings can provide the impacted populace time
64 to take appropriate action to help prevent loss of life and potentially reduce property

65 damage (e.g., Sene 2013). Empirical evidence exists that such warnings do decrease flash
66 flood fatalities (e.g., DeKay and McClelland 1993). The first half of the proposed causality
67 chain, however, requires more explanation on how flash flood warning decisions are made.

68 In the U.S., operational flash flood warning decisions rely primarily on the concept of
69 flash flood guidance (FFG; Ostrowski et al. 2003). Based on basin hydrological models
70 with soil moisture and stream flow as initial conditions, FFG outputs rainfall accumulation
71 needed in 1-, 3-, 6-, or 12-hour periods to cause flash flood conditions on a typical small
72 stream or urban area in the region of interest. There are different types of FFG models used
73 at different weather forecast offices (WFOs)—lumped FFG, gridded FFG, distributed FFG,
74 flash flood potential index. However, regardless of type, the basic idea is that the forecaster
75 looks for accumulated quantitative precipitation estimation (QPE) to exceed the FFG rain
76 accumulation threshold in a given catchment basin when issuing a flash flood warning;
77 decision support tools such as the flash flood monitoring and prediction (FFMP) system
78 aid the forecaster in this process (Clark et al. 2014).

79 By definition, flash floods occur within six hours of the causative event (NWS 2019).
80 Thus, when the cause is heavy rain, in order for the WFO to issue a timely flash flood
81 warning, forecasters mostly utilize multisensor precipitation estimator (MPE) products for
82 comparison with FFG thresholds. (Waiting for flow level measurements from stream
83 gauges delays the decision, and, in any case, many potential flash flood areas are in
84 ungauged headwaters.) MPE ingests radar, rain gauge, and geostationary satellite data; rain
85 gauge data are used to help correct biases in the radar and satellite estimates. The dominant
86 MPE contributor is radar QPE, while satellite QPE is mainly used to fill gaps in radar
87 coverage (Kitzmilller et al. 2013). Also, with finer spatial resolution hydrological models

88 becoming feasible for operational use, the value of highly resolved rainfall estimates from
89 radars is expected to rise in the future (Gourley et al. 2014). Forecasters have started to
90 consult short-term rainfall nowcasts as well (Ahnert et al. 2012).

91 The flash flood warning decision process, therefore, depends on the accuracy of the
92 FFG and MPE products. FFG threshold errors are dependent on FFG type and are specific
93 to each catchment basin. There are various sources of MPE errors, including those for radar
94 QPE such as choice of algorithm, radar calibration, and rain gauge density (e.g., Cecinati
95 et al. 2017). The situation is further complicated by the fact that the WFOs do not utilize a
96 uniform set of data products and decision support tools. To analyze the impacts of input
97 data errors on flash flood warning performance would require an in-depth case study at a
98 particular WFO using a detailed hydrological model of a catchment basin—this is not
99 conducive to a national-scale statistical analysis.

100 In this study, we took a simple approach. Since poor radar coverage is a significant
101 source of radar QPE error (Rogalus and Ogden 2012; Kurdzo et al. 2018), we hypothesized
102 that flash flood warning performance would depend on radar coverage, even without taking
103 into account the other error sources in the warning decision process—this is proved true in
104 sections 2d and 2e. By linking radar coverage directly to warning performance, we
105 bypassed the very complex problem of characterizing MPE and FFG product errors,
106 considerably simplifying the analysis. We believe a clear statistical signal was extractable
107 due to the large number of cases nationwide used in the analysis.

108 To summarize briefly, we propose an original geospatial model for monetizing flash
109 flood casualty reduction benefits of a meteorological radar network. This analysis, along
110 with the earlier tornado benefit effort (CK19), was conducted for the National Oceanic and

111 Atmospheric Administration (NOAA) as part of a larger program that is studying future
112 radar systems beyond the Weather Surveillance Radar-1988 Doppler (WSR-88D).
113 Benefits must be weighed carefully against costs in considering advanced technologies
114 such as active phased array radars (Weber et al. 2007; Zrnić et al. 2007) and/or a denser
115 network of smaller radars (McLaughlin et al. 2009).

116 In dealing with the complex nature of the problem, we employed only the bare
117 essentials in objectively modeling the radar effects. In contrast to detailed hydrological
118 simulation or survey-based case studies, we relied on the power of large data sets to yield
119 statistically meaningful results with simple models. We made conservative choices when
120 there was uncertainty. Statistically insignificant variables were disregarded. Our
121 geographic scope was limited to the contiguous United States (CONUS), as that is where
122 most of the relevant data were available and wide variation in radar coverage exists.

123

124 **2. Model Development**

125 Following the successful radar network benefit modeling approach of CK19 for
126 tornadoes, we sought to establish statistical relationships using historical flash flood data
127 between (1) radar coverage metrics and flash flood warning performance, and (2) flash
128 flood warning performance and casualty rate. With these two links established, the flash
129 flood casualty rate could be computed geospatially for any given weather radar network.
130 With casualty monetized, the difference between a baseline case (e.g., the current WSR-
131 88D network) and a hypothetical radar network would yield the benefit (or loss). The
132 methodologies used throughout follows closely those used by CK19.

133 To provide a visual aid for understanding both the model development process and the
134 model usage, Figure 1 gives high-level block diagram views of these procedures. The
135 reader is encouraged to refer back to this figure while reading the detailed explanations in
136 the following sections.

137

138 *a. Analysis data source and time period*

139 We needed to use as much data as possible to achieve statistically significant results.
140 At the same time, however, we had to maintain uniform conditions for unbiased regression
141 results. Our primary source was the U.S. Flash Flood Observation Database (Gourley et al.
142 2013) compiled by the Flooded Locations and Simulated Hydrographs (FLASH) project
143 (Gourley et al. 2017). Although the earliest-processed NWS storm reports in the FLASH
144 database are from 2006, the official transition from county-based flash flood reporting (a
145 single point indicating an event somewhere in the county) to polygon-based reporting did
146 not occur until 1 October 2007. Thus, we limited our analysis period to begin on this
147 transition date (the transition from county-based to storm-based warnings also took place
148 on the same day). Furthermore, because the FLASH storm report database only extended
149 to July 2013, we supplemented that data with storm reports pulled from NOAA’s National
150 Center for Environmental Information (<https://www.ncdc.noaa.gov/stormevents/>) up to 31
151 December 2018, which we then processed to match the content and format of the FLASH
152 data. This yielded about twelve years of flash flood data to analyze. Only reports with an
153 associated cause of “heavy rain” were retained.

154 Storm warning data for the matching period were obtained from the Iowa
155 Environmental Mesonet NWS Watch/Warnings archive

156 (<https://mesonet.agron.iastate.edu/request/gis/watchwarn.phtml>). If any part of the flash
157 flood polygon was inside the warning polygon and if any segment of the flash flood time
158 span overlapped the warning valid interval, then the warning was considered a hit;
159 otherwise, it was labeled a false alarm. The lead time for a hit was computed as the
160 beginning time of the flash flood minus the initial warning issuance time. For the
161 remainder of the paper, we will refer to the fraction of flash floods with warning
162 interchangeably with probability of detection (POD) for brevity.

163

164 *b. Radar coverage metrics*

165 The radar observational characteristics important for QPE accuracy are vertical
166 coverage, horizontal resolution, and availability of dual-polarization products (Kurdzo et
167 al. 2019). The data update rate might also have an impact on flash flood warning
168 performance. An ongoing study aims to answer this question, and early results show that
169 QPE from faster radar scans can improve agreement between measured and simulated
170 stream gauge levels during flash floods (Wen et al. 2018).

171 With vertical coverage, the most crucial aspect is the radar antenna beam's minimum
172 height above ground level (AGL), since the aim of QPE is to match the rainfall
173 measurement at the surface. However, information aloft is also useful to forecasters for
174 determining location of the radar bright band (Austin and Bemis 1950), regions of mixed-
175 phase precipitation (Balakrishnan and Znić 1990), and for ingest to QPE correction
176 algorithms such as Vertical Profiles of Reflectivity (VPR; Kirstetter et al. 2010).
177 Additionally, future uses such as Quasi-Vertical Profiles (QVP; Ryzhkov et al. 2016) may
178 be of use to forecasters for determining rainfall rates. Thus, we decided to employ the same

179 coverage metric, fraction of vertical volume observed (FVO) between 0 to 20 kft AGL
180 (1 kft = 304.8 m), as we did for the CK19 tornado study. The rationale for picking 20 kft
181 as the FVO ceiling is that the current WSR-88D network (on which we base the statistical
182 analysis) has essentially perfect coverage above 20 kft (Figure 2); therefore, no information
183 content is added by moving the ceiling higher, whereas moving it lower progressively
184 eliminates actual deficiencies in coverage from consideration. FVO includes the effects of
185 the Earth's curvature, terrain blockage, and the radar's overhead "cone of silence" due to
186 its limited elevation scanning angle, so it is a convenient and effective metric.

187 Details of the beam blockage calculations are given by Cho (2015). The minimum
188 and maximum elevation coverage angles were assumed to be 0° and 20° , roughly
189 corresponding to the bottom and top sides of the main antenna lobe at the WSR-88D scan
190 angle limits of 0.5° and 19.5° . These limits are approximations, as the maximum elevation
191 angles vary for different volume coverage patterns (VCPs) and the minimum angle has
192 recently been lowered slightly at a few high-altitude sites (Steadman and Brown 2007).

193 Cross-radial horizontal resolution (CHR), which is approximately range times
194 azimuthal angular resolution, is also relevant. (Along-range horizontal resolution is
195 constant everywhere for monostatic radars, so it is not of value here.) Azimuthal angular
196 resolution is dependent on dwell length and antenna beamwidth (Zrnich and Doviak 1976).
197 The WSR-88D beamwidth is just under 1° . Presently, it has a "superresolution" mode that
198 outputs data every 0.5° ; however, the effective angular resolution is about 1° based on the
199 antenna beamwidth and time-series data window (Torres and Curtis 2006). Taking all this
200 into account, we took the angular resolution to be 1° for the analysis period. Consequently,
201 for the current WSR-88D, the resulting CHR is functionally the same as the distance from

202 the radar. CHR could become a more meaningful performance metric, since future radar
203 networks may have varying angular resolutions—for example, with a mix of powerful
204 narrow-beam radars augmented by gap-filling broad-beam systems (Chandrasekar et al.
205 2012), or with the angle-dependent resolution of fixed planar phased arrays (Weber et al.
206 2017).

207 During the analysis period (October 2007 to December 2018), the WSR-88D CONUS
208 network underwent two relevant changes. First, a new radar was added at Langley Hill,
209 Washington in September 2011. Second, the network was upgraded from single
210 polarization to dual polarization. To address the first change, we produced two sets of FVO
211 and CHR maps corresponding to before and after the Langley Hill deployment. For the
212 second network change, we conducted our analysis over the entire database timespan as
213 well as the single polarization period and the post-dual-polarization upgrade period. To
214 ensure that there would be no cross-contamination between the two polarization eras, the
215 end of the single polarization period was marked by the first operational CONUS
216 deployment of dual polarization (8 March 2011), and the start of the dual polarization
217 period was marked by the completion of CONUS deployment (16 May 2013).

218 Although we included Terminal Doppler Weather Radars (TDWRs) in our earlier
219 analysis for tornadoes, because we determined that forecasters utilize TDWR data for
220 tornado warning decisions, we did not include them for flash floods, since TDWRs are not
221 used for QPE purposes.

222

223 *c. Mapping flash flood event to corresponding basin*

224 Flooding location is different from the place where the causative rain falls. In order
225 to study the relationship between the quality of radar coverage (which affects QPE
226 accuracy) and flash flood warning performance, we had to match each flood event to the
227 appropriate upstream catchment basin. To do this we utilized the United States Geological
228 Survey (USGS) National Hydrography Dataset Plus (NHDPlus;
229 <https://water.usgs.gov/GIS/metadata/usgswrd/XML/streamgagebasins.xml>). This database
230 contains the location of 19 031 stream gauges with corresponding catchment basin
231 boundaries.

232 For each flood event, we searched for a stream gauge located inside the event polygon,
233 and computed the mean radar coverage metric over the matching source basin (Figure 3).
234 If more than one stream gauge was found inside the event polygon, then the radar coverage
235 metric means were computed over all corresponding basins. If no stream gauge was
236 situated in the polygon, then we looked for the nearest stream gauge; if the distance to the
237 mean polygon latitude-longitude coordinate was less than 10 km, the stream gauge match
238 was accepted. (This means the matched stream gauge was even closer to the polygon
239 border.) With this procedure, 24 236 flash flood events were matched to source basins over
240 the analysis period. All the analyses conducted on flash floods described in the rest of this
241 paper were based on this set of events.

242

243 *d. Detection probability dependence on radar coverage*

244 Flash flood warning POD statistics were computed vs. the basin-averaged radar
245 coverage parameters (Figure 4, top row). For FVO, the data were binned based on
246 cumulative distribution percentage intervals of [0, 1], (1, 5], (5, 25], (25, 50], (50, 75], and

247 (75, 100]. For CHR, the data were binned based on cumulative distribution percentage
248 intervals of [0, 25], (25, 50], (50, 75], (75, 95], (95, 99], and (99, 100]. The asymmetric
249 interval distributions help draw out the steep change regimes where data were sparse. Note
250 that the abscissa values plotted do not correspond to the center of the data bins—instead,
251 they are the actual means of the binned FVO or CHR data. The vertical and horizontal
252 error bars denote the 95% confidence intervals along both dimensions (see CK19 for
253 further details).

254 Flash flood POD unambiguously increases with FVO and decreases with CHR. This
255 is a very important result, because it connects better radar coverage to flash flood warning
256 performance improvement, and allows a continuous functional mapping between the two.
257 (This result is also consistent with a prior study that showed a positive dependence of POD
258 on WSR-88D low-level coverage over NWS WFO areas; Meléndez et al. 2018.) We
259 modeled these relationships by two-segment linear fits with input uncertainty in both
260 dimensions using the “fitexy” function from Numerical Recipes (Press et al. 1992). Fitting
261 results are given in Table 1, where a is the y intercept, b is the slope, σ_a and σ_b are the
262 standard deviations of a and b , χ^2 is the fitted chi-squared value, and Q is the goodness-of-
263 fit probability.

264 As can be seen in the POD vs. FVO plot of Figure 4, there is a discernible change in
265 slope between FVO = 0.7 and 0.8. (The slope change is more gradual in the FAR vs. FVO
266 plot.) If we assume that all of the observation loss occurs at the bottom of the volume
267 (which is true except for the small fraction attributable to the radar cone of silence at the
268 top of the volume), $FVO = (20 \text{ kft} - \text{minimum observation height}) / 20 \text{ kft}$. Note, then, that
269 FVO of 0.7 and 0.8 approximately correspond to floors of 6000 and 4000 ft AGL. Thus, if

270 one had to pick one altitude as the “critical floor” for radar coverage with respect to flash
271 flood warning performance, it would be ~5000 ft AGL; the top left plot in Figure 2
272 corresponds to this height.

273 Flash flood detection can be defined based on only positive lead times or all lead times
274 (including zero and negative lead times). We decided on the latter, because the casualty
275 regression statistics were better with all lead times included (section 2h). For a measure of
276 model sensitivity, we also did the analysis with detections defined with only positive lead
277 times. As expected, the primary impact of excluding zero and negative lead times was to
278 reduce the POD values; however, POD still increased with FVO, POD decreased with
279 CHR, and the fits remained significant.

280 We also tried combining the FVO and CHR relationships in the flash flood POD model
281 via weighted additions of the two relationships. The mean-squared sums of the difference
282 between data and model were minimized to obtain the optimal weighting. The error was
283 minimized with a 0.86 weight on the FVO relationship and a 0.14 weight on the CHR
284 relationship.

285

286 *e. False alarm ratio dependence on radar coverage*

287 To compute flash flood warning false alarm ratio (FAR) statistics vs. the radar
288 coverage metrics, we matched each warning to the relevant catchment basin(s) following
289 the method outlined in section 2c for flood events. In this case, however, the event polygon
290 depicted in Figure 3 is replaced by the warning polygon. With this procedure, 32 438 flash
291 flood warnings were matched to source basins over the analysis period. (All the analyses
292 conducted on flash floods described in the rest of this paper were based on this set of

293 warnings.) The radar coverage parameter values were then averaged over the
294 corresponding basin boundaries.

295 The resulting FAR vs basin-averaged radar coverage parameters plots are shown in
296 the bottom row of Figure 4. For FVO, the data were binned based on cumulative
297 distribution percentage intervals of [0, 1], (1, 10], (10, 25], (25, 50], (50, 75], and (75, 100].
298 For CHR, the data were binned based on cumulative distribution percentage intervals of
299 [0, 25], (25, 50], (50, 75], (75, 90], (90, 99], and (99, 100].

300 FAR clearly decreases with FVO and increases with CHR. This result is consistent
301 with an earlier analysis that showed a negative dependence of FAR on WSR-88D low-level
302 coverage over NWS WFO areas (Meléndez et al. 2018). Unfortunately, however, because
303 the casualty regression analysis did not yield a statistically meaningful relationship
304 between historical FAR and casualty rate (section 2h), we were not able to exploit this clear
305 dependency of flash flood FAR on radar coverage for our benefit model. (Hence, linear fits
306 to the bottom row plots in Figure 4 are not given.)

307 Note that we did not use a combined warning performance metric such as the critical
308 success index (CSI) due to a couple of reasons. First, POD could be applied to the casualty
309 regression model (section 2h) on a per-event basis via the binary warning presence
310 variable, whereas FAR and CSI could not. Second, for a geospatial mapping of historical
311 warning performance (for use by the regression model), the mismatch in spatial boundaries
312 for computing POD (event polygons) and FAR (warning polygons) presented a problem in
313 combining them for CSI; hence, only FAR was tried for that purpose.

314 As for warning lead time, our analysis did show a positive correlation between
315 increased radar coverage and lead time. However, because flash flood lead time did not

316 correlate negatively with casualty rate (section 2h), we could not include it as part of our
317 benefit model.

318

319 *f. Impact of dual polarization upgrade*

320 To investigate the impact of the WSR-88D dual polarization upgrade on flash flood
321 warning performance, we computed the mean CONUS POD and FAR over two periods:
322 (1) 1 October 2007 to 7 March 2011 and (2) 16 May 2013 to 31 December 2018. As
323 explained in section 2b, these dates were chosen based on the first operational CONUS
324 dual polarization deployment (8 March 2011) and the completion of the CONUS upgrade
325 deployment (16 May 2013). Table 2 lists the corresponding POD and FAR values for these
326 periods as well as for the entire analysis period. The plus/minus values indicate the 95%
327 confidence intervals for the means.

328 The mean flash flood warning values did not yield statistically meaningful differences
329 between the single polarization and dual polarization eras. This stands in contrast to case
330 studies that showed dramatic improvement in flash flood warning performance when the
331 nation's meteorological radar network was upgraded to the WSR-88D from the WSR-57
332 and WSR-74 (Polger et al. 1994). One of the challenges with QPE in the dual-polarization
333 era is the ongoing difficulty with differential reflectivity (Z_{DR}) calibration, leading to
334 difficulties obtaining consistent QPE results for use in the flash-flood warning process
335 (Ryzhkov et al. 2005). As a result, the NWS has approved the transition to an R(A)
336 algorithm based on specific attenuation (Snow 2017). The R(A) technique uses a slope of
337 the Z_{DR}/Z (horizontal reflectivity factor), meaning that constant offsets in Z_{DR} across the
338 tilt/volume theoretically will not cause as much of an error in QPE (Cocks et al. 2018;

339 Ryzhkov and Zrnić 2019). Initial results of the R(A) algorithm have shown promise
340 relative to the R(Z, Z_{DR}) method when polarimetric bias is introduced (Kurdzo et al. 2019).
341 It is possible that the eventual use of R(A) will impact our results in the future.

342 The good news is that the flash flood warning vs. radar coverage statistics as
343 exemplified by the Figure 4 plots were quite stable over the single and dual polarization
344 periods. This was another confirmation that these relationships are meaningful and robust,
345 and further justified their use in the benefit estimation model.

346

347 *g. Non-flash flood warnings vs. radar coverage*

348 Although this study focused on flash floods (and they account for the majority of
349 flood-related fatalities; Ashley and Ashley 2008), we took the opportunity to investigate
350 the relationship between radar coverage and non-flash flood warning performance. Using
351 the same procedure employed for the flash flood analysis yielded no discernible coherent
352 relationship between POD and FVO or CHR, and between FAR and FVO or CHR. These
353 null results are perhaps not surprising, given that warning decisions for longer-term events
354 must be based primarily on model forecast data, and the importance of QPE to the flood
355 forecasting process diminishes with increasing time horizon as stream gauge data and
356 quantitative precipitation forecast (QPF) become more relevant (e.g., Hudlow et al. 1984).
357 These results preclude the addition of non-flash floods to our radar network benefit model.

358

359 *h. Casualty dependence on flash flood warning*

360 With the causal link between radar coverage and flash flood warning performance
361 clearly established, we proceed to discuss the connection between flash flood warnings and

362 casualty rates. Among the factors that are thought to affect flash flood casualty rate are
363 population, time of day, building type, catchment basin size, water flow velocity and depth,
364 rate of water level rise, and warning lead time, and they appear to interact in various ways
365 to impact casualty rates. For example, while most casualty events occur around headwater
366 catchments in rural areas (because flash floods are generated by the rapid response time of
367 small basins to heavy rainfall), when they do occur downstream in urban areas, the casualty
368 rates are higher (Špitalar et al. 2014). The same article reports that while flash flood
369 occurrence in the U.S. peaks around 1700 local time (LT), the per-event casualty rate
370 reaches a maximum at 2100 LT, hinting at the importance of human factors such as
371 inability to see in the dark for those outside. We refer the reader to informative past reviews
372 on this topic (e.g., Jonkman et al. 2008; Smith and Rahman 2016). For the purposes of
373 developing a radar network benefit model, only variables that could be geospatially
374 characterized were considered. Temporal predictors like season and time of day were
375 excluded, since they were not germane to our time-independent benefit model. However,
376 in the future, the model could be extended to capture temporal effects.

377 The flash flood casualty variance was more than twenty times larger than the mean
378 statistics over our analysis period. Thus, instead of a Poisson distribution that is often used
379 for counting statistics, we adopted a negative binomial distribution model for the casualty
380 count,

381

$$382 \quad C \sim \text{NegBin}(\mu, \theta), \quad (1)$$

383

384 for our casualty regression analysis, where μ is the distribution mean, and θ is the
385 dispersion parameter. The regression model then was a linear combination of candidate
386 predictor variables set equal to $\ln \mu$. This is the same scheme that we used for the CK19
387 tornado study.

388 At this point, casualties were not divided between fatalities and injuries. Since the vast
389 number of events have zero (no casualty) outcomes, increasing the number of non-zero
390 outcome cases by aggregating fatalities and injuries improves statistical robustness. While
391 the database includes direct and indirect casualties separately, we only used direct
392 casualties in our analysis, because we sought the tightest causal bond between flash floods
393 and their effects on people. In the monetization stage (section 2i), we parsed the model
394 results into fatalities and two types of injuries based on historical averages.

395 The predictor variables that we tried in the regression analysis were (1) logarithm of
396 the population, (2) fraction of population in mobile housing, (3) historical flash flood
397 warning FAR, (4) catchment basin size (as a proxy for basin response time), (5) flood
398 flashiness, (6) flash flood warning presence (binary—0 or 1), and (7) flash flood warning
399 lead time. (1), (2), and (3) were averaged over the flood event polygon. The predictor
400 variables were tested both individually and in combination to elucidate any cross-
401 correlation effects. We also tried FVO and CHR (averaged over the source basins) as
402 casualty predictors to see if a direct link could be established between radar coverage and
403 casualty rate, but there was no meaningful statistical relationship, consistent with the
404 findings of Meléndez et al. (2018).

405 We acquired population data from the Center for International Earth Science
406 Information Network (CIESIN 2017) with latitude-longitude spacing that matched our 30-

407 arcsec model grid resolution. Measured population for 2005, 2010, 2015 were available, as
408 well as projected population for 2020; linear interpolation yielded corresponding data for
409 the other years. In a nod to statistics that showed most flash flood fatalities occurring while
410 people were away from their residences (predominantly while driving, but also during
411 hiking, camping, etc.; Terti et al. 2017), we set a floor of 1 in the population field
412 everywhere. Also, in cases where the event casualty count exceeded the population in the
413 event polygon, the population was set to the casualty count for logical consistency.
414 Otherwise, we relied on a general spatial correlation between residential population and
415 transient mobile population.

416 Flood flashiness, defined as the peak flow above flood stage divided by the product of
417 basin area and time from flood stage exceedance to peak flow (Saharia et al. 2017), was
418 considered, because it seemed to hold promise as a predictor of flash flood casualty rate.
419 Since the NWS storm events database did not contain quantitative data on water flow or
420 depth, we computed flashiness from USGS streamflow measurements (2016V1;
421 <https://blog.nssl.noaa.gov/flash/database/database-2016v1/>) archived under the FLASH
422 database (Gourley et al. 2013). However, in comparing the NWS flash flood events to the
423 USGS streamflow measurements by time and location, only a small fraction of the former
424 found matched with the latter. Therefore, any casualty regression results that included
425 flashiness as a predictor variable was handicapped by the reduction in input data points.

426 The fraction of the population living in mobile housing was an effective predictor
427 variable for tornado casualties (CK19). Intuitively, one might expect the heightened
428 vulnerability of mobile housing to be washed away by flood waters to be a factor in casualty
429 rate. In fact, about a third of building-related flash flood casualties was estimated to have

430 occurred in mobile homes (Terti et al. 2017). Mobile housing and trailer parks are also
431 often located near rivers (Marrero 1979), while a proposed flash flood severity index
432 codifies the sweeping away of mobile homes as a category-defining characteristic
433 (Schroeder et al. 2016). The gridded fraction of the population in mobile housing were
434 computed from data obtained from the American Community Survey database for 2015
435 (USCB 2016) and the Decennial Census for 2000 (Manson et al. 2018). We combined the
436 population in the “mobile home” and “boat, RV, van, etc.” categories to arrive at the mobile
437 housing population, which was normalized by the total population in each census block
438 group to yield the fraction of population in mobile housing. We sampled and mapped this
439 data to our 30-arcsec latitude-longitude model grid. See CK19 for further details. In the
440 regression analysis, linearly interpolated maps (between 2000 and 2015) were used for the
441 years 2007–2014, and the 2015 map (Figure 5) was used for 2015–2018.

442 For the negative binomial regression analysis, we utilized the “glm.nb” function from
443 the open software package R (<https://www.R-project.org/>). An exhaustive search of
444 predictor combinations yielded a clear winner based on statistical reliability. The best
445 regression fit statistics were obtained by keeping only population (P), fraction of
446 population in mobile housing (M), and warning presence (W) in the statistical model,

447

$$448 \quad \ln \mu = \alpha \ln P + \beta M + \gamma W + k , \quad (2)$$

449

450 where k is the intercept constant, and α , β , and γ are the regression coefficients. For the
451 definition of warning presence we tried including all lead times vs. only positive lead times,
452 and the better result was obtained by including all lead times. The fit results are given in

453 Table 3. The probability of the “null hypothesis being true” for each predictor was less than
454 0.0003, much smaller than the typically used threshold of 0.05. Additionally, comparison
455 of the casualty regression relation with and without each predictor via degree-of-freedom
456 chi-square tests showed that each variable was a statistically significant predictor.

457 Applying the same flash flood events input data to (2) with the estimated coefficients
458 gave a casualty count of 681, which is reasonably close to the actual count of 631. The
459 presence of a flash flood warning reduces casualty rate by 44% according to this model.

460

461 *i. Monetizing casualties*

462 The value of a statistical life (VSL) is commonly used to monetize casualties in benefit
463 analyses. As we did previously (CK19), we followed the guidance of the Department of
464 Transportation (DOT 2016), which established a VSL of \$9.6 million (M) in 2015 dollars.
465 To update the value to 2019 dollars, we used the DOT’s equation,

466

467
$$VSL_T = VSL_0 \frac{CPI_T}{CPI_0} \left(\frac{MUWE_T}{MUWE_0} \right)^q, \quad (3)$$

468

469 where CPI is the consumer price index, MUWE is the median usual weekly earnings, q is
470 income elasticity, and the subscripts T and 0 signify updated base year and original base
471 year. We got $CPI_T/CPI_0 = 1.08$ (https://www.bls.gov/data/inflation_calculator.htm) and
472 $MUWE_T/MUWE_0 = 1.12$ (<https://www.bls.gov/cps/cpswktabs.htm>) from the U.S. Bureau
473 of Labor Statistics database, for a baseline of January 2015 and updated time of January
474 2019. Taking the DOT’s recommended value of $q = 1$ yielded a 2019 VSL of \$11.6M.

475 We did not distinguish between fatalities and injuries in our casualty regression model
476 as explained in section 2h. We used the actual mean ratio calculated over the analysis
477 period to parse the model output into the two casualty types, which yielded 61% fatalities
478 and 39% injuries.

479 Injuries were monetized as fractions of VSL, relying on a Federal Emergency
480 Management Administration (FEMA) formulation (FEMA 2009) specifying injuries
481 requiring hospitalization as level 4, and injuries resulting in treatment and release as level
482 2. With the DOT setting level 4 injury cost at $0.266 \times \text{VSL}$ and level 2 injury cost at
483 $0.047 \times \text{VSL}$ (DOT 2016), these costs are \$3.09M and \$0.545M, respectively, in 2019
484 dollars.

485 Because the flood event database does not categorize injuries by severity, we scoured
486 the Internet for papers and news reports that contained flash flood injury outcome
487 information. We found usable reports on twelve events between 1956 and 2018 with 3336
488 total injuries, with the count being dominated by the 9 June 1972 Rapid City, South Dakota
489 event. In order to avoid being biased by one event, we computed the ratio of injury types
490 for each event then took the mean of the ratios. The result was 43% for injuries requiring
491 hospitalization vs. 57% for injuries that were treated and released.

492

493 *j. CONUS grid computation*

494 All the individual model components can now be integrated to generate mean annual
495 CONUS flash flood casualty cost. The modeled casualty rate (per year, per grid cell) is
496 given by

497

498
$$R_{ij}^{F,H,R} = Y^{F,H,R} [r_{ij}(1)B_{ij} + r_{ij}(0)(1 - B_{ij})]O_{ij} , \quad (4)$$

499

500 where B is the probability of warning per flash flood (POD), O is the flash flood occurrence
 501 rate, i and j are the latitude and longitude grid indices, and the superscripts indicate fatal
 502 (F), injured—hospitalized (H), and injured—treated and released (R). The grid cell size is
 503 $1/120^\circ \times 1/120^\circ$. The casualty type fractions are broken down as

504

505
$$Y^F = f , \quad (5)$$

506
$$Y^H = (1 - f)h , \text{ and} \quad (6)$$

507
$$Y^R = (1 - f)(1 - h) , \quad (7)$$

508

509 where f is the fatality fraction and h is the fraction of injured that are hospitalized. From
 510 (2) we get the casualty rate per flash flood,

511

512
$$r_{ij}(W) = \exp[\alpha \ln(P_{ij}) + \beta M_{ij} + \gamma W + k] , \quad (8)$$

513

514 with ($W = 1$) and without ($W = 0$) a flash flood warning.

515 To generate the flash flood POD map, we applied the Table 1 fitted parameters to the
 516 radar network FVO and CHR maps and summed them with weights given in section 2d.
 517 However, a geospatial mapping was needed, because equation (4) is computed over the
 518 grid cells of flash flood occurrence, not radar observation of the source rainfall. Thus, we
 519 mapped every CONUS grid cell to the nearest USGS NHDPlus stream gauge (Figure 6),
 520 which was mapped to the corresponding source basin grid cells. The modeled flash flood

521 POD computed based on mean radar FVO and CHR over the source basins were then able
522 to be mapped onto the flash flood occurrence areas. The modeled POD values were
523 computed from $0.86 \times \text{POD}(\text{FVO}) + 0.14 \times \text{POD}(\text{CHR})$. $\text{POD}(\text{FVO})$ and $\text{POD}(\text{CHR})$ were
524 calculated using the piecewise-linear relationships given by the a (y intercept) and b (slope)
525 coefficients in Table 1 (and expressed by the red lines in Figure 4). The resulting flash
526 flood POD map for the current WSR-88D network is shown in Figure 7.

527 The mean annual flash flood occurrence rate was computed for each CONUS grid cell
528 using the NWS storm database over the period 2006–2018. Earlier NWS data were not
529 used, because the cause of flooding was not recorded. In order to obtain better coverage
530 and statistics (since flash floods occur relatively rarely and the NWS database is not a
531 comprehensive source), we also computed occurrence rate with the USGS streamflow
532 measurements that date back to 1936, based on exceedance of the action stage. Since these
533 observations came from single point locations, we counted the floods as having occurred
534 in the four closest grid cells. In joining the results from the two disparate data sets, we took
535 the greater occurrence rate value in each grid cell instead of combining them in order to
536 avoid double counting. For visualization purposes, Figure 8 shows the mean annual
537 CONUS flash flood occurrence rate density mapped from the event locations to the
538 corresponding source basins. Without this mapping, the occurrence rates at the actual
539 locations are too small to be discernible at the national level—they appear as sparse dots
540 on the CONUS map.

541 We arrived at the predicted CONUS flash flood casualty rate parsed by casualty type
542 by summing (4) over all grid indices. The total estimated annual CONUS flash flood

543 casualty cost was obtained by multiplying the individual casualty rates with the
544 corresponding casualty type costs and summing.

545

546 **3. Example results**

547 In order to estimate the value provided by the current radar network, as well as the
548 remaining benefit pool, we computed modeled flash flood casualty costs for three basic
549 scenarios: the current WSR-88D network, no radar coverage, and perfect WSR-88D-like
550 coverage. No radar coverage was simulated by setting $FVO = 0$ and $CHR = \infty$ everywhere.
551 Perfect WSR-88D-like coverage was simulated by setting $FVO = 1$ and $CHR = 0$
552 everywhere.

553 Table 4 lists the flash flood casualty estimates for all scenarios and the actual average
554 annual casualty rates. The agreement between the baseline model estimates and the actual
555 casualty rates is very good, especially with the median actual rates. Table 5 gives the
556 corresponding flash flood casualty costs in 2019 dollars.

557 Differences from the current baseline are provided in the “Delta baseline” columns of
558 Tables 4 and 5. This shows that today’s WSR-88D network provides over \$300M dollars
559 in flash flood benefits annually compared to a CONUS without weather radars. Perfect
560 radar coverage of the CONUS yields a benefit of only \$13M yr^{-1} over the baseline. The
561 remaining benefit pool with respect to improved coverage is, therefore, quite modest for
562 flash flood casualty reduction, especially compared to the tornado case, which has an order
563 of magnitude larger benefit pool (CK19). Evidently, for the purposes of QPE to support
564 flash flood warning decisions, the coverage provided by the current baseline is quite good.

565 To estimate the benefit provided by flash flood warnings independent of radar
566 coverage, we also ran the model on a CONUS with no flash flood warnings and with 100%
567 warnings (Tables 4 and 5). The results indicate that over \$390M yr⁻¹ benefit is realized by
568 the current flash flood warning system compared to a world without warnings, and the
569 remaining benefit pool for warnings is about \$69M yr⁻¹—this corresponds to the
570 hypothetical situation of having 100% warning on flash floods. (The impact of lead time
571 and false alarm ratio improvements could not be modeled, because these variables were
572 not statistically significant predictors of casualty rate.) This value also corresponds to the
573 upper-bound benefit for radars, since, in principle, improvements to radar QPE through
574 non-coverage aspects such as rapid scanning and product algorithm enhancements could
575 help push flash flood POD toward 100%.

576 Because the average fraction of injured that are hospitalized ($h = 0.43$) used in the
577 model was based on a small number of cases, we tested the model sensitivity by changing
578 this parameter to 0.25 and 0.75. For $h = 0.25$, the magnitude of the benefits in Tables 4 and
579 5 decreased by 2%, and for $h = 0.75$, the magnitude of the benefits increased by 4%. Thus,
580 the model appears to be fairly stable with respect to even large variances in this parameter.

581 Figure 9 shows geospatially the casualty cost density difference between perfect radar
582 coverage and the WSR-88D network. The cost densities were mapped from the casualty
583 locations to the source basins of the flash floods in order to show where improvements in
584 radar coverage may help with respect to flash flood casualty reduction. Impacts from both
585 the flash flood occurrence rate (Figure 8) and modeled warning probability (Figure 7) are
586 discernible in Figure 9. For example, the mountainous region west of Charlottesville,
587 Virginia has both fairly high flash flood occurrence rate and low modeled warning

588 probability (corresponding to a radar coverage gap noticeable in the Figure 2, 5000-ft AGL
589 plot), resulting in a larger benefit pool. The poor low-altitude radar coverage in the
590 Mountain West, however, does not generally lead to a greater benefit pool, except in areas
591 with more frequent occurrence of flash floods (and perhaps population).

592 There are, of course, a number of cautionary notes regarding this analysis. First is the
593 incomplete nature of the flash flood data. For example, the NWS flood event data are based
594 on reports by human observers, and floods that occurred in remote locations or had no
595 impact on people may have been missed. Fortunately, the benefits are accumulated in areas
596 with people, so biases in the event data may not greatly affect the modeled benefit
597 estimates. Rapid housing development in remote areas prone to flooding, however, might
598 lead to slight localized underestimates of future benefits.

599 Second, there are factors that influence the flash flood warning decision process not
600 accounted for in our model, such as the skill of individual forecasters, procedural
601 heterogeneity across regional forecast centers, evolution of the QPE and FFG products,
602 FFG errors, density of rain gauge network, availability of other data sources, storm type,
603 and basin hydrological features. Also, temporal evolution of a basin, such as when a fire
604 decimates vegetation, can greatly affect runoff response time. However, as the statistical
605 stability of the radar-coverage-to-warning-performance relationship over the pre- and post-
606 dual-polarization eras attests, variances due to these other factors appear to largely get
607 averaged out over the large number of data points ingested in the analysis.

608 Finally, the circumstances of flash flood casualties are very complex and difficult to
609 model statistically. Many flash flood fatalities in the U.S. occur while the victim is away
610 from their residence, which cannot be precisely characterized with population data. It is

611 difficult to capture factors like real-time access to flash flood warnings and likelihood of
612 response (Knocke and Kolivras 2007; Parker et al. 2009; Morss et al. 2016), while data on
613 event characteristics such as flow speed and depth are not universally available. In our
614 casualty regression analysis, we considered potential causative factors with data available
615 geospatially on a national basis, and discarded those that were not statistically reliable
616 predictors. The resulting regression model is necessarily a simple one, but, again, the large
617 number of data points used in the analysis provides a high level of statistical robustness
618 that would not be available in a more detailed case study.

619

620 **4. Summary discussion**

621 We constructed a geospatial model for computing meteorological radar network
622 benefits for flash flood casualty reduction. We showed unambiguously that better radar
623 coverage of the causative rainfall leads to improved flash flood warning statistics. We also
624 established that the casualty rate decreases by 44% when a flash flood warning is present.
625 Combining these two effects, the model was able to generate benefit estimates on a high-
626 resolution spatial grid. The model can work on an arbitrary radar network configuration.

627 Our model showed that today's WSR-88D network provides over \$300M yr⁻¹ in flash
628 flood casualty reduction. There is a modest remaining benefit pool of \$13M yr⁻¹ for
629 coverage improvements, which is indicative of the effective coverage provided for this
630 purpose by the current weather radar network. Inclusive of all aspects of flash flood
631 warning POD improvements, including better radar QPE, the maximum benefit pool is
632 \$69M yr⁻¹.

633 A radar benefit model could not be established for non-flash floods, since our analysis
634 did not yield a meaningful relationship between radar coverage and warning performance.
635 This negative result was not entirely a surprise, given that warning decisions for longer-
636 term events must be based primarily on model forecast data, and the importance of QPE to
637 the flood forecasting process diminishes with increasing time horizon as stream gauge data
638 and QPF become more relevant.

639 Potential benefits from flash flood property damage reduction could be worth
640 investigating, although loss mitigation options may be limited in this scenario (relocating
641 vehicles, moving valuables from basements and first floors to upper levels, etc.). Also,
642 damage reduction is expected to be less for shorter lead time flash flood events compared
643 to longer lead time non-flash flood events (Day 1970). A preliminary analysis using
644 population as a proxy for property value did not yield any statistically meaningful
645 relationship between flash flood warning performance and property damage. For a proper
646 study, geospatial data of real estate property type and value as well as vehicle count would
647 likely be needed.

648

649 *Acknowledgments.* We would like to sincerely thank the following people: Chris
650 Miller for acquiring and processing the housing-type data; Angie Locknar, for gathering
651 news reports of flash flood injury type statistics; J. J. Gourley, Pierre Kirstetter, and Berry
652 Wen, for providing valuable technical guidance; and Kurt Hondl and Mark Weber, for
653 supporting this project. This paper has been approved for public release: distribution is
654 unlimited. This material is based upon work supported by the National Oceanic and
655 Atmospheric Administration under Air Force Contract FA8702-15-D-0001. Any opinions,

656 findings, conclusions, or recommendations expressed in this material are those of the
657 authors and do not necessarily reflect the views of the National Oceanic and Atmospheric
658 Administration.
659

REFERENCES

660

661

662 Ahnert, P., E. Clark, P. Corrigan, and H. White, 2012: National Weather Service flash flood
 663 warning services. *26th Conf. on Hydrology*, New Orleans, LA, Amer. Meteor. Soc.,

664 TJ7.2, 16 pp.,

665 https://ams.confex.com/ams/92Annual/webprogram/Manuscript/Paper199494/marfc_ahnert_ams_final.pdf.

667 Ashley, S. T., and W. S. Ashley, 2008: Flood fatalities in the United States. *J. Appl. Meteor. Climatol.*, **47**, 805–818, <https://doi.org/10.1175/2007JAMC1611.1>.

669 Austin, P. M., and A. C. Bemis, 1950: A quantitative study of the “bright band” in radar
 670 precipitation echoes. *J. Meteor.*, **7**, 145–151, [https://doi.org/10.1175/1520-0469\(1950\)007<0145:AQSOTB>2.0.CO;2](https://doi.org/10.1175/1520-0469(1950)007<0145:AQSOTB>2.0.CO;2).

672 Balakrishnan, N., and D. S. Zrnić, 1990: Estimation of rain and hail rates in mixed-phase
 673 precipitation. *J. Atmos. Sci.*, **47**, 565–583, [https://doi.org/10.1175/1520-0469\(1990\)047<0565:EORAGR>2.0.CO;2](https://doi.org/10.1175/1520-0469(1990)047<0565:EORAGR>2.0.CO;2).

675 Cecinati, F., M. A. Rico-Ramirez, G. B. M. Heuvelink, and D. Han, 2017: Representing
 676 radar rainfall uncertainty with ensembles based on a time-variant geostatistical error
 677 modelling approach. *J. Hydrol.*, **548**, 391–405,
 678 <https://doi.org/10.1016/j.jhydrol.2017.02.053>.

679 Chandrasekar, V., H. Chen, and M. Maki, 2012: Urban flash flood applications of high-
 680 resolution rainfall estimation by X-band dual-polarization radar network. *Proc. SPIE*,
 681 **8523**, 85230K, <https://doi.org/10.1117/12.977602>.

682 Cho, J. Y. N., 2015: Revised Multifunction Phased Array Radar (MPAR) network siting
683 analysis. Project Rep. ATC-425, MIT Lincoln Laboratory, 84 pp.,
684 [https://www.ll.mit.edu/sites/default/files/publication/doc/2018-05/Cho_2015_ATC-](https://www.ll.mit.edu/sites/default/files/publication/doc/2018-05/Cho_2015_ATC-425.pdf)
685 [425.pdf](https://www.ll.mit.edu/sites/default/files/publication/doc/2018-05/Cho_2015_ATC-425.pdf).

686 —, and J. M. Kurdzo, 2019a: Monetized weather radar network benefits for tornado cost
687 reduction. Project Rep. NOAA-35, MIT Lincoln Laboratory, 88 pp.,
688 [https://www.ll.mit.edu/sites/default/files/publication/doc/monetized-weather-radar-](https://www.ll.mit.edu/sites/default/files/publication/doc/monetized-weather-radar-network-benefits-cho-noaa-35.pdf)
689 [network-benefits-cho-noaa-35.pdf](https://www.ll.mit.edu/sites/default/files/publication/doc/monetized-weather-radar-network-benefits-cho-noaa-35.pdf).

690 —, and J. M. Kurdzo, 2019b: Weather radar network benefit model for tornadoes. *J.*
691 *Appl. Meteor. Climatol.*, **58**, 971–987, <https://doi.org/10.1175/JAMC-D-18-0205.1>.

692 CIESIN, 2017: Gridded Population of the World, ver. 4 (GPWv4): Population density, rev.
693 10. NASA Socioeconomic Data and Applications Center, Center for International
694 Earth Science Information Network, Columbia University, Palisades, NY,
695 <https://doi.org/10.7927/H4DZ068D>.

696 Clark, R. A., J. J. Gourley, Z. L. Flamig, Y. Hong, and E. Clark, 2014: CONUS-wide
697 evaluation of National Weather Service flash flood guidance products. *Wea.*
698 *Forecasting*, **29**, 377–392, <https://doi.org/10.1175/WAF-D-12-00124.1>.

699 Cocks, S. B., L. Tang, Y. Wang, J. Zhang, A. Ryzhkov, P. Zhang, and K. W. Howard,
700 2018: MRMS precipitation estimates using specific attenuation. *32nd Conf. on*
701 *Hydrology*, Austin, TX, Amer. Meteor. Soc.,
702 <https://ams.confex.com/ams/98Annual/webprogram/Paper335167.html>.

703 Day, H. J., 1970: Flood warning benefit evaluation—Susquehanna River basin (urban
704 residences). ESSA Technical Memorandum WBTM HYDRO 10, Department of
705 Commerce, Silver Spring, MD, 42 pp.

706 DeKay, M. L., and D. H. McClelland, 1993: Predicting loss of life in cases of dam failure
707 and flash flood. *Risk Anal.*, **13**, 193–205.

708 DOT, 2016: Guidance on treatment of the economic value of a statistical life (VSL) in U.S.
709 Department of Transportation Analyses—2016 adjustment. Memorandum to
710 secretarial officers and modal administrators, DOT Office of the Secretary of
711 Transportation, 13 pp.,
712 [https://cms.dot.gov/sites/dot.gov/files/docs/2016%20Revised%20Value%20of%20a](https://cms.dot.gov/sites/dot.gov/files/docs/2016%20Revised%20Value%20of%20a%20Statistical%20Life%20Guidance.pdf)
713 [%20Statistical%20Life%20Guidance.pdf](https://cms.dot.gov/sites/dot.gov/files/docs/2016%20Revised%20Value%20of%20a%20Statistical%20Life%20Guidance.pdf).

714 Gourley, J. J., Y. Hong, Z. L. Flamig, A. Arthur, R. A. Clark, M. Calianno, I. Ruin, T.
715 Ortel, M. E. Wiczorek, E. Clark, P.-E. Kirstetter, and W. F. Krajewski, 2013: A
716 unified flash flood database over the US. *Bull. Amer. Meteor. Soc.*, **94**, 799–805,
717 <https://doi.org/10.1175/BAMS-D-12-00198.1>.

718 ———, Z. L. Flamig, Y. Hong, and K. W. Howard, 2014: Evaluation of past, present and
719 future tools for radar-based flash-flood prediction in the USA. *Hydro. Sci. J.*, **59**,
720 1377–1398, <https://doi.org/10.1080/02626667.2014.919391>.

721 ———, Z. Flamig, H. Vergara, P. Kirstetter, R. Clark III, E. Argyle, A. Arthur, S. Martinaitis,
722 G. Terti, J. Erlingis, Y. Hong, and K. Howard, 2017: The Flooded Locations And
723 Simulated Hydrographs (FLASH) project: Improving the tools for flash flood
724 monitoring and prediction across the United States. *Bull. Amer. Meteor. Soc.*, **98**, 361–
725 372. <https://doi.org/10.1175/BAMS-D-15-00247.1>.

726 Hudlow, M. D., R. K. Farnsworth, and P. R. Ahnert, 1984: NEXRAD technical
727 requirements for precipitation estimation and accompanying economic benefits.
728 Hydro Technical Note 4, NWS Office of Hydrology, Silver Spring, MD, 49 pp.

729 Jonkman, S. N., J. K. Vrijling, A. C. W. M. Vrouwenvelder, 2008: Methods for the
730 estimation of loss of life due to floods: A literature review and a proposal for a new
731 method. *Nat. Hazards*, **46**, 353–389, <https://doi.org/10.1007/s11069-008-9227-5>.

732 Kirstetter, P., H. Andrieu, G. Delrieu, and B. Boudevillain, 2010: Identification of vertical
733 profiles of reflectivity for correction of volumetric radar data using rainfall
734 classification. *J. Appl. Meteor. Climatol.*, **49**, 2167–2180,
735 <https://doi.org/10.1175/2010JAMC2369.1>.

736 Kitzmiller, D., D. Miller, R. Fulton, and F. Ding, 2013. Radar and multisensor precipitation
737 estimation techniques in National Weather Service hydrologic operations. *J. Hydrol.*
738 *Eng.*, **18**, 133–142, [http://dx.doi.org/10.1061/\(ASCE\)HE.1943-5584.0000523](http://dx.doi.org/10.1061/(ASCE)HE.1943-5584.0000523).

739 Knocke, E. T., and K. N. Kolivras, 2007: Flash flood awareness in southwest Virginia. *Risk*
740 *Anal.*, **27**, 155–169, <https://doi.org/10.1111/j.1539-6924.2006.00866.x>.

741 Kurdzo, J. M., E. F. Clemons, J. Y. N. Cho, P. L. Heinselman, and N. Yussouf, 2018:
742 Quantification of QPE performance based on SENSR network design possibilities.
743 *Proc. 2018 IEEE Radar Conf.*, Oklahoma City, OK, Institute of Electrical and
744 Electronics Engineers, 169–174, <https://doi.org/10.1109/RADAR.2018.8378551>.

745 ———, E. F. Joback, J. Y. N. Cho, and P.-E. Kirstetter, 2019: QPE accuracy benefits for
746 weather radar network design. *J. Appl. Meteor. Climatol.*, submitted.

747 Manson, S., J. Schroeder, D. Van Riper, and S. Ruggles, 2018: IPUMS National Historical
748 Geographic Information System, version 13.0. University of Minnesota, accessed 11
749 June 2018, <https://doi.org/10.18128/D050.V13.0>.

750 Marrero, J., 1979: Danger: Flash floods. *Weatherwise*, **32**, 34–37,
751 <https://doi.org/10.1080/00431672.1979.9930069>.

752 McLaughlin, D., and Coauthors, 2009: Short-wavelength technology and the potential for
753 distributed networks of small radar systems. *Bull. Amer. Meteor. Soc.*, **90**, 1797–1818,
754 <https://doi.org/10.1175/2009BAMS2507.1>.

755 Meléndez, D., K. Abshire, and J. Sokich, 2018: NEXRAD weather radar coverage and
756 National Weather Service warning performance. *AGU 2018 Fall Meeting*,
757 Washington, DC, Amer. Geophys. Union, A11K-2394,
758 <https://doi.org/10.1002/essoar.10500135.1>.

759 Morss, R. E., K. J. Mulder, J. K. Lazo, and J. L. Demuth, 2016: How do people perceive,
760 understand, and anticipate responding to flash flood risks and warnings? Results from
761 a public survey in Boulder, Colorado, USA. *J. Hydrol.*, **541**, 649–664,
762 <https://doi.org/10.1016/j.jhydrol.2015.11.047>.

763 NOAA, 2019: Natural hazard statistics. NWS Office of Climate, Water, and Weather
764 Services, <http://www.nws.noaa.gov/om/hazstats.shtml>.

765 NWS, cited 2019: National Weather Service glossary,
766 <http://w1.weather.gov/glossary/index.php>.

767 Ostrowski, J., et al., 2003: Flash flood guidance improvement team: Final report. NWS
768 Office of Hydrologic Development, 47 pp.,
769 <http://www.nws.noaa.gov/ohd/rfcdev/docs/ffgitreport.pdf>.

770 Parker, D. J., S. J. Priest, and S. M. Tapsell, 2009: Understanding and enhancing the
771 public's behavioural response to flood warning information. *Meteorol. Appl.*, **16**, 103–
772 114, <https://doi.org/10.1002/met.119>.

773 Polger, P. D., B. S. Goldsmith, R. C. Przywarty, and J. S. Bocchieri, 1994: National
774 Weather Service warning performance based on the WSR-88D. *Bull. Amer. Meteor.*
775 *Soc.*, **75**, 203–214, [https://doi.org/10.1175/1520-
776 0477\(1994\)075%3C0203:NWSWPB%3E2.0.CO;2](https://doi.org/10.1175/1520-0477(1994)075%3C0203:NWSWPB%3E2.0.CO;2).

777 Press, W. H., S. A. Teukolsky, W. T. Vetterling, and B. P. Flannery, 1992: *Numerical*
778 *Recipes in C: The Art of Scientific Computing*. 2nd Ed. Cambridge University Press,
779 994 pp.

780 Rogalus, M. J., III, and F. L. Ogden, 2012: Spatial assessment of five years of WSR-88D
781 data over the Mississippi River basin and its estimation bias around rain gauge sites.
782 *J. Hydrol. Eng.*, **18**, 212–218, [https://doi.org/10.1061/\(ASCE\)HE.1943-
783 5584.0000636](https://doi.org/10.1061/(ASCE)HE.1943-5584.0000636).

784 Ryzhkov, A. V., S. E. Giangrande, V. M. Melnikov, and T. J. Schuur, 2005: Calibration
785 issues of dual-polarization radar measurements. *J. Atmos. Oceanic Technol.*, **22**,
786 1138–1155, <https://doi.org/10.1175/JTECH1772.1>.

787 ———, and D. S. Zrnić, 2019: *Radar Polarimetry for Weather Observations*. Springer, 486
788 pp., <https://doi.org/10.1007/978-3-030-05093-1>.

789 Saharia, M., P. E. Kirstetter, H. Vergara, J. J. Gourley, Y. Hong, Y., and M. Giroud, 2017:
790 Mapping flash flood severity in the United States. *J. Hydrometeor.*, **18**, 397–411,
791 <https://doi.org/10.1175/JHM-D-16-0082.1>.

792 Saunders, M. E., K. D. Ash, and J. M. Collins, 2018: Usefulness of the United States
793 National Weather Service radar display as rated by website users. *Wea. Climate Soc.*,
794 **10**, 673–691, <https://doi.org/10.1175/WCAS-D-17-0108.1>.

795 Schroeder, A. J., J. J. Gourley, J. Hardy, J. J. Henderson, P. Parhi, V. Rahmani, V., and M.
796 J. Taraldsen, 2016: The development of a flash flood severity index. *J. Hydrol.*, **541**,
797 523–532, <https://doi.org/10.1016/j.jhydrol.2016.04.005>.

798 Sene, K., 2013: *Flash Floods: Forecasting and Warning*. Springer, 386 pp.,
799 <https://doi.org/10.1007/978-94-007-5164-4>.

800 Smith, G. P., and P. F. Rahman, 2016: Approaches for estimating flood fatalities relevant
801 to floodplain management. WRL Tech. Rep. 2015/09, Water Research Laboratory,
802 University of New South Wales, Manly Vale, Australia, 52 pp.,
803 [https://knowledge.aidr.org.au/media/2333/wrl-approches-for-estimating-flood-](https://knowledge.aidr.org.au/media/2333/wrl-approches-for-estimating-flood-fatalities-september-2016.pdf)
804 [fatalities-september-2016.pdf](https://knowledge.aidr.org.au/media/2333/wrl-approches-for-estimating-flood-fatalities-september-2016.pdf).

805 Snow, J., 2017: Recommendation of R(A) technique for QPE. Memorandum, NEXRAD
806 Technical Advisory Committee, 1 p.,
807 <https://www.roc.noaa.gov/WSR88D/PublicDocs/TAC/2017/February2017NEXRAD>
808 [TAC-Specific%20Attenuation%20QPE%20Decision.pdf](https://www.roc.noaa.gov/WSR88D/PublicDocs/TAC/2017/February2017NEXRAD).

809 Špitalar, M., J. J. Gourley, C. Lutoff, P.-E. Kirstetter, M. Brilly, and N. Carr, 2014:
810 Analysis of flash flood parameters and human impacts in the US from 2006 to 2012.
811 *J. Hydrol.*, **519**, 863–870, <https://doi.org/10.1016/j.jhydrol.2014.07.004>.

812 Steadman, R. M, and R. A. Brown, 2007: Plan for testing the feasibility of site-specific
813 scanning strategies for WSR-88Ds. *23rd Conf. on Interactive Information Processing*

814 *Systems (IIPS)*, San Antonio, TX, Amer. Meteor. Soc., 5B.3,
815 <https://ams.confex.com/ams/pdfpapers/117708.pdf>.

816 Stensrud, D. J., et al., 2009: Convective-scale warn-on-forecast system: A vision for 2020.
817 *Bull. Amer. Meteor. Soc.*, **90**, 1487–1500, <https://doi.org/10.1175/2009BAMS2795.1>.

818 Terti, G., I. Ruin, S. Anquetin, and J. J. Gourley, 2017: A situation-based analysis of flash
819 flood fatalities in the United States. *Bull. Amer. Meteor. Soc.*, **98**, 333–345,
820 <https://doi.org/10.1175/BAMS-D-15-00276.1>.

821 Torres, S., and C. Curtis, 2006: Design considerations for improved tornado detection using
822 superresolution data on the NEXRAD network. *Third European Conf. on Radar*
823 *Meteorology and Hydrology (ERAD)*, Barcelona, Spain, Copernicus,
824 [http://citeseerx.ist.psu.edu/viewdoc/download?doi=10.1.1.738.9413&rep=rep1&type](http://citeseerx.ist.psu.edu/viewdoc/download?doi=10.1.1.738.9413&rep=rep1&type=pdf)
825 [=pdf](http://citeseerx.ist.psu.edu/viewdoc/download?doi=10.1.1.738.9413&rep=rep1&type=pdf).

826 USCB, 2016: B25033: Total population in occupied housing units by tenure by units in
827 structure. 2011–2015 American Community Survey 5-Year Estimates, U. S. Census
828 Bureau, accessed 11 June 2018, <http://factfinder2.census.gov>.

829 Weber, M. E., J. Y. N. Cho, J. S. Herd, J. M. Flavin, W. E. Benner, and G. S. Torok, 2007:
830 The next-generation multimission US surveillance radar network. *Bull. Amer. Meteor.*
831 *Soc.*, **88**, 1739–1751, <https://doi.org/10.1175/BAMS-88-11-1739>.

832 ———, J. Y. N. Cho, and H. G. Thomas, 2017: Command and control for multifunction
833 phased array radar. *IEEE Trans. Geosci. Remote Sens.*, **55**, 5899–5912,
834 <https://doi.org/10.1109/TGRS.2017.2716935>.

835 Wen, B., T. Schuur, C. Kuster, and H. Vergara, 2018: Advancing flash flooding early
836 warning using a rapid-scan polarimetric radar observations. *9th Int. Precipitation*

837 *Working Group (IPWG) Workshop*, Seoul, South Korea, Coordination Group for
838 Meteorological Satellites, [http://www.isac.cnr.it/~ipwg/meetings/seoul-](http://www.isac.cnr.it/~ipwg/meetings/seoul-2018/Orals/15-3_Wen.pdf)
839 [2018/Orals/15-3_Wen.pdf](http://www.isac.cnr.it/~ipwg/meetings/seoul-2018/Orals/15-3_Wen.pdf).
840 Zrnić, D. S. and R. J. Doviak, 1976: Effective antenna pattern of scanning radars. *IEEE*
841 *Trans. Aerosp. Electron. Syst.*, **AES-12**, 551–555,
842 <https://doi.org/10.1109/TAES.1976.308254>.
843 ———, J. F. Kimpel, D. E. Forsyth, A. Shapiro, G. Crain, R. Ferek, J. Heimmer, W. Benner,
844 F. T. J. McNellis, and R. J. Vogt, 2007: Agile-beam phased array radar for weather
845 observations. *Bull. Amer. Meteor. Soc.*, **88**, 1753–1766,
846 <https://doi.org/10.1175/BAMS-88-11-1753>.
847

848

TABLE CAPTIONS

849

850

Table 1. POD vs. radar coverage parameters linear fit results.

851

Table 2. Mean CONUS flash flood POD and FAR.

852

Table 3. Flash flood casualty model regression results.

853

Table 4. Annual CONUS flash flood casualty estimates. Actual average injured

854

counts are totals, not broken out by injury type.

855

Table 5. Annual CONUS flash flood casualty cost estimates.

856

FIGURE CAPTIONS

857

858

859 Fig. 1. Development and usage block diagrams of the radar network flash flood
860 casualty cost model. Input data are indicated by gray rectangles, intermediate data products
861 by green rectangles, and final monetized cost output by a blue rectangle. Computational
862 model units are shown as orange ovals.

863 Fig. 2. WSR-88D coverage at the indicated height slices.

864 Fig. 3. Illustration of how a flood event is matched to the source basin.

865 Fig. 4. Plots of (top left) flash flood POD vs. FVO, (top right) flash flood POD vs.
866 CHR, (bottom left) flash flood FAR vs. FVO, and (bottom right) flash flood FAR vs. CHR.
867 Solid red lines are linear fits to the data.

868 Fig. 5. Fraction of population living in mobile housing as derived from the 2015
869 American Community Survey data given at the census block group level.

870 Fig. 6. Areas associated with nearest USGS NHDPlus stream gauge colored according
871 to the logarithm of the number of grid points enclosed.

872 Fig. 7. Modeled flash flood warning probability for the current WSR-88D network.

873 Fig. 8. Mean annual flash flood occurrence rate density with the rates mapped from
874 the event locations to the corresponding source basins. Computed based on combined
875 USGS and NWS flash flood data from 1936 to 2018.

876 Fig. 9. Modeled annual flash flood casualty cost density difference between the
877 current WSR-88D network and perfect radar coverage.

878
879

Table 1. POD vs. radar coverage parameters linear fit results.

Parameter Segment	FVO		CHR	
	Low FVO	High FVO	Low CHR	High CHR
a	0.11	0.68	0.88	1.1
b	0.89	0.20	-1.4×10^{-5}	-1.2×10^{-4}
σ_a	0.12	0.074	0.011	0.075
σ_b	0.15	0.084	8.1×10^{-6}	3.2×10^{-5}
χ^2	0.037	0.13	1.2	0.89
Q	0.85	0.94	0.54	0.35

880
881

882
883

Table 2. Mean CONUS flash flood POD and FAR.

Period	2007-10-1 to 2018-12-31	2007-10-1 to 2011-3-7	2013-5-16 to 2018-12-31
POD (all lead times)	0.853 ± 0.005	0.857 ± 0.008	0.853 ± 0.006
POD (positive lead times only)	0.774 ± 0.005	0.776 ± 0.010	0.775 ± 0.007
Number of points averaged (POD)	24 236	7097	13 408
FAR	0.452 ± 0.005	0.434 ± 0.010	0.453 ± 0.007
Number of points averaged (FAR)	32 438	9729	17 518

884
885

886
887
888

Table 3. Flash flood casualty model regression results.

Parameter	Estimate	Std. error	z	Pr ($> z $)
α	0.166	0.020	8.13	4×10^{-16}
β	2.20	0.435	5.05	4×10^{-7}
γ	-0.572	0.160	-3.59	3×10^{-4}
k	-4.58	0.206	-22.2	$< 2 \times 10^{-16}$
θ	0.105	7.16×10^{-4}	N/A	N/A

889
890

891 Table 4. Annual CONUS flash flood casualty estimates. Actual average injured counts
 892 are totals, not broken out by injury type.
 893

Scenario	Fatal	Injured (hospitalized)	Injured (treated and released)	Total	Delta baseline
WSR-88D	52.6	14.5	19.2	86.3	—
No radar coverage	77.6	21.4	28.4	127.4	41.1
Perfect coverage	51.5	14.2	18.9	84.6	-1.7
0% warned	83.6	23.1	30.6	137.2	50.9
100% warned	47.2	13.0	17.3	77.4	-8.9
Actual mean (2007– 2018)	63 ± 10	41 ± 15		104 ± 20	N/A
Actual median (2007–2018)	59 ± 7	23 ± 8		86 ± 13	N/A

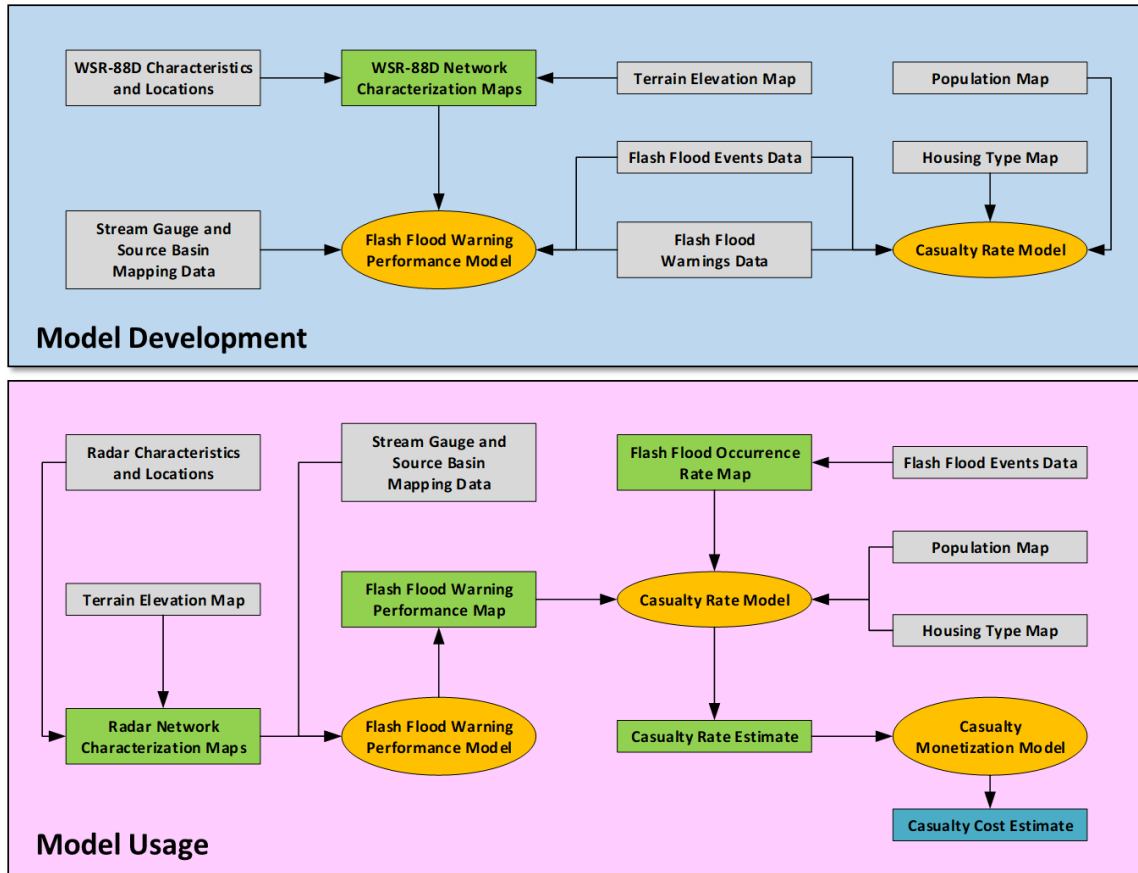
894
 895

896
897

Table 5. Annual CONUS flash flood casualty cost estimates.

Scenario	Fatal (\$M)	Injured (hospitalized) (\$M)	Injured (treated and released) (\$M)	Total (\$M)	Delta baseline (\$M)
WSR-88D	609.9	44.8	10.5	665.2	—
No radar coverage	899.8	66.1	15.5	981.3	316.1
Perfect coverage	597.7	43.9	10.3	651.9	-13.3
0% warned	969.6	71.2	16.7	1057.4	392.2
100% warned	547.0	40.2	9.4	596.5	-68.7

898
899



900

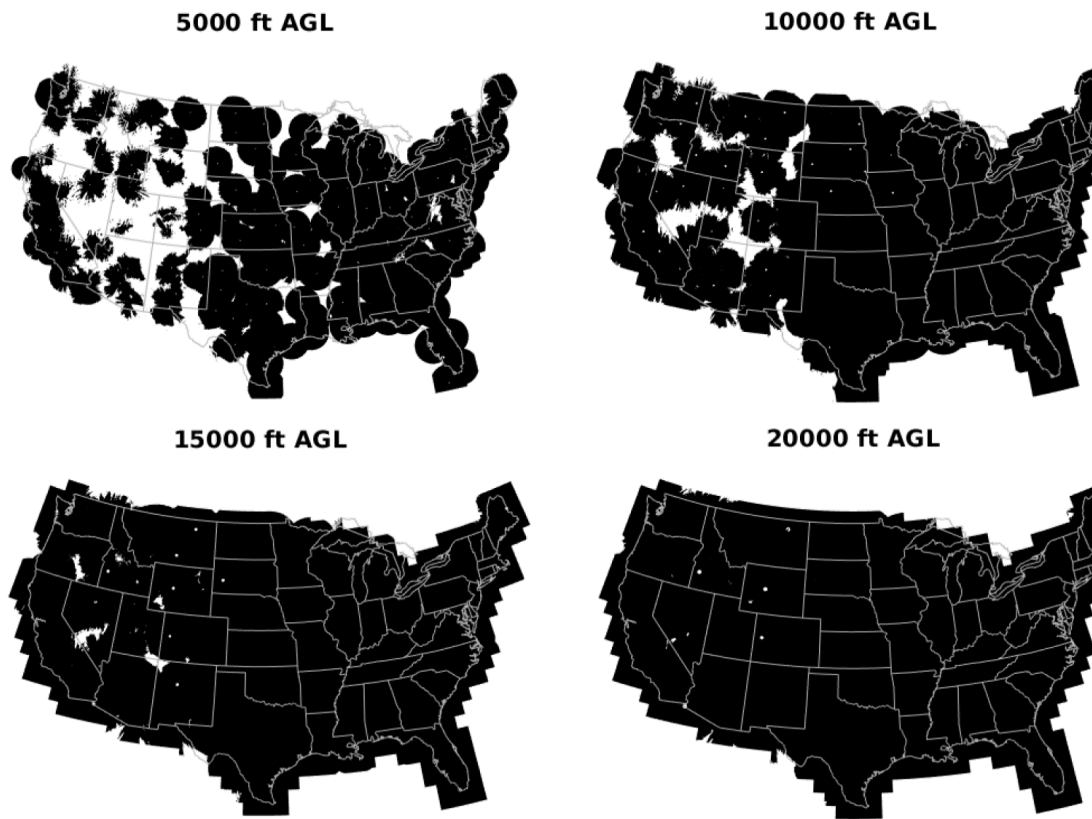
901 Fig. 1. Development and usage block diagrams of the radar network flash flood casualty

902 cost model. Input data are indicated by gray rectangles, intermediate data products by green

903 rectangles, and final monetized cost output by a blue rectangle. Computational model units

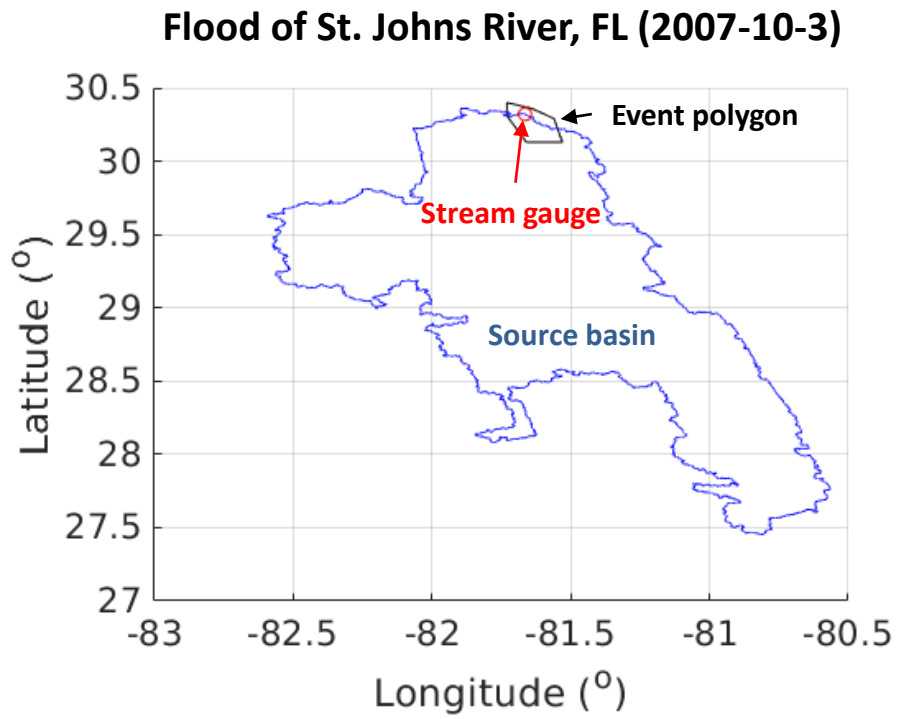
904 are shown as orange ovals.

905
906



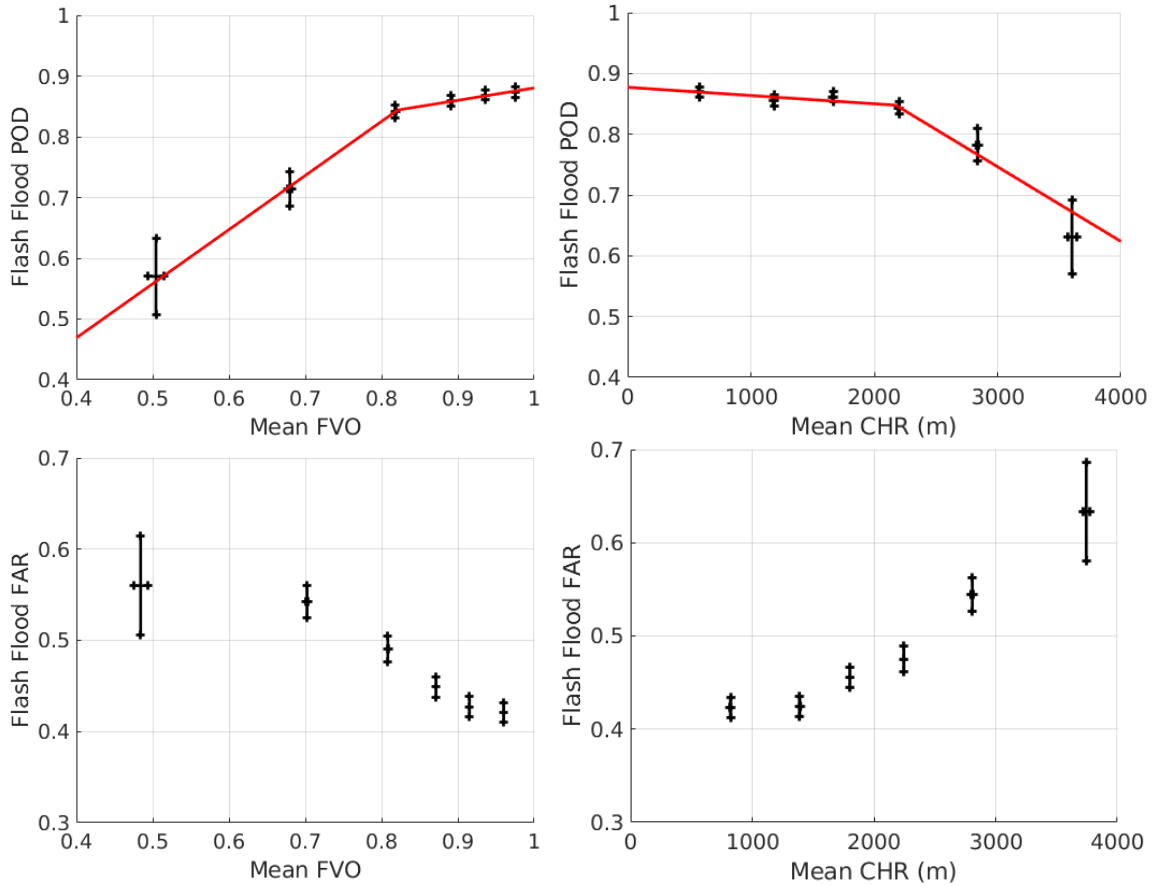
907
908

Fig. 2. WSR-88D coverage at the indicated height slices.



909
910
911

Fig. 3. Illustration of how a flood event is matched to the source basin.



912

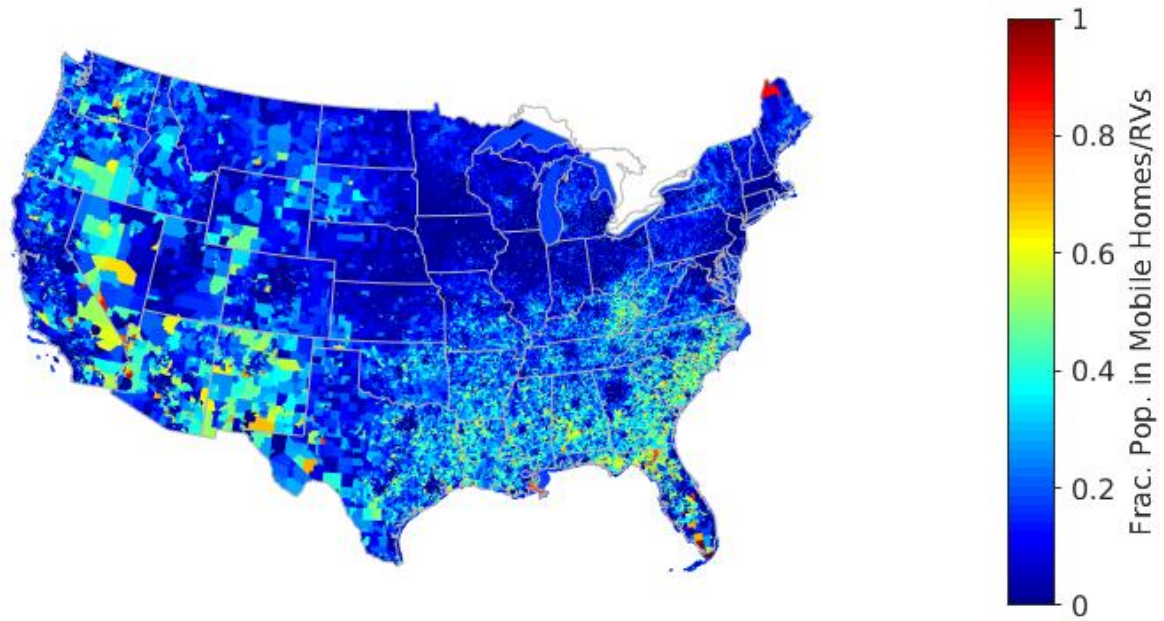
913

Fig. 4. Plots of (top left) flash flood POD vs. FVO, (top right) flash flood POD vs. CHR, (bottom left) flash flood FAR vs. FVO, and (bottom right) flash flood FAR vs. CHR. Solid red lines are linear fits to the data.

914

915

916



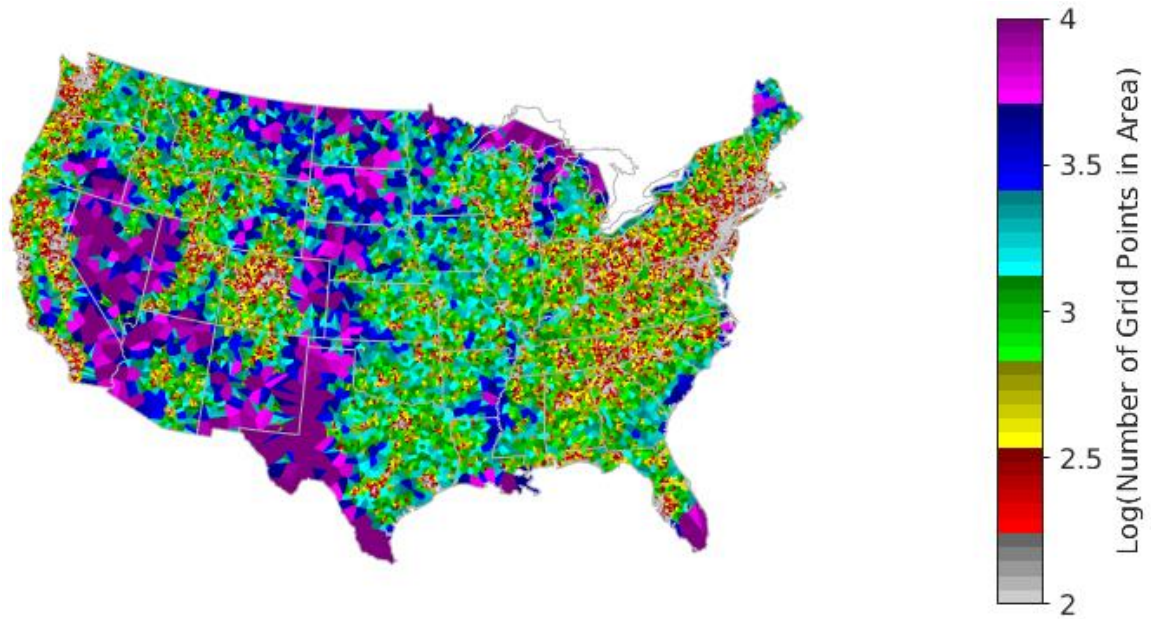
917

918

919

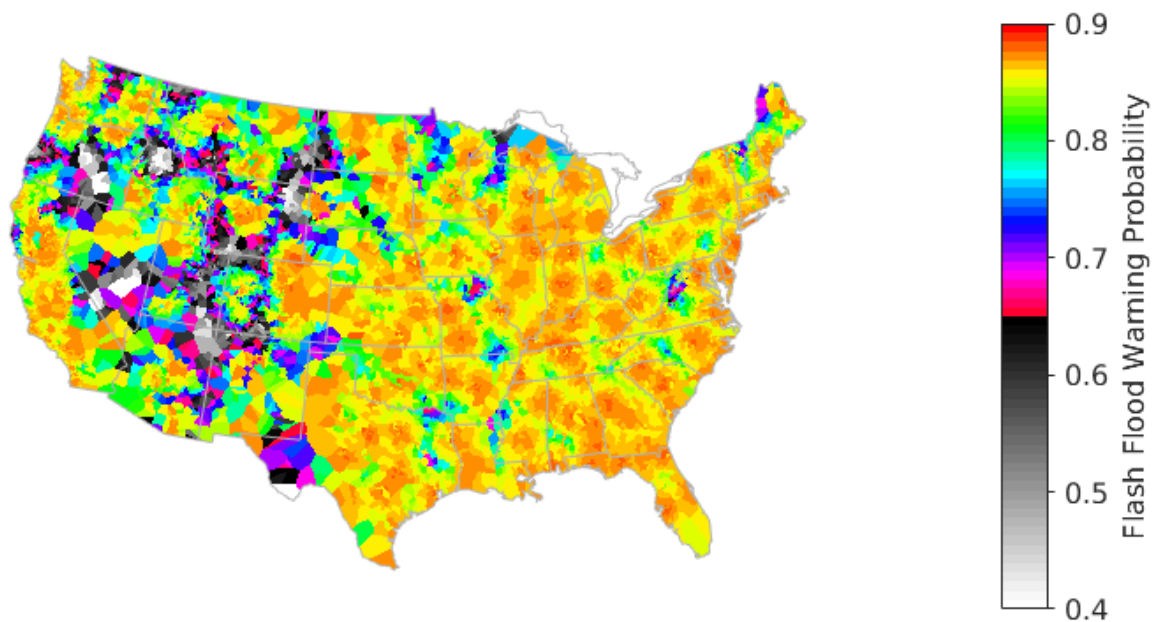
920

Fig. 5. Fraction of population living in mobile housing as derived from the 2015 American Community Survey data given at the census block group level.



921
922
923
924

Fig. 6. Areas associated with nearest USGS NHDPlus stream gauge colored according to the logarithm of the number of grid points enclosed.



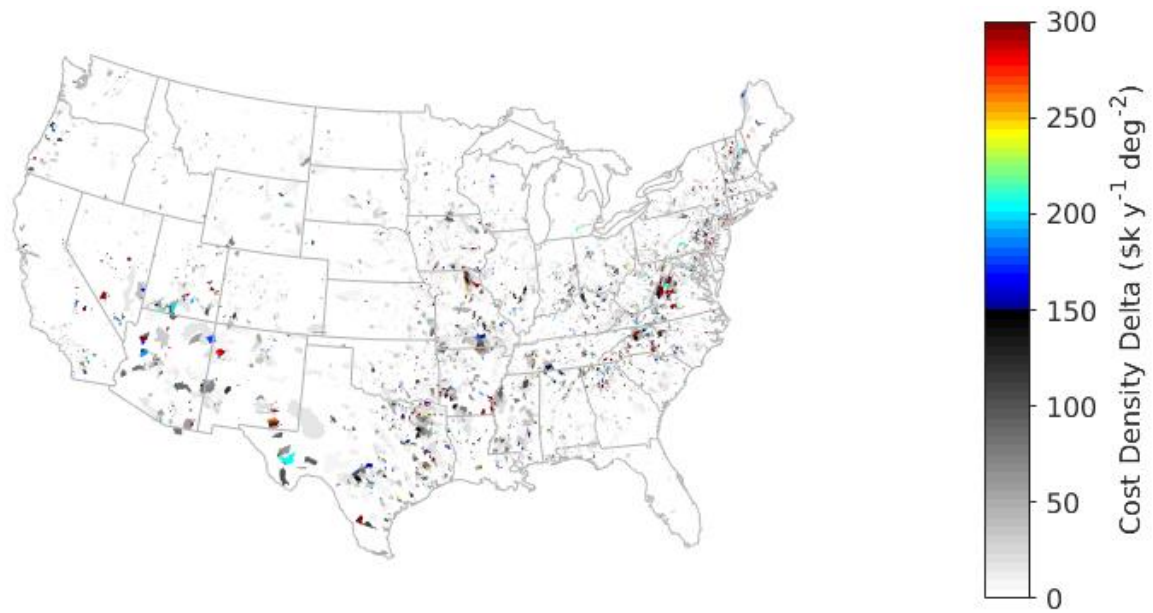
925
926
927

Fig. 7. Modeled flash flood warning probability for the current WSR-88D network.



928
929
930
931
932

Fig. 8. Mean annual flash flood occurrence rate density with the rates mapped from the event locations to the corresponding source basins. Computed based on combined USGS and NWS flash flood data from 1936 to 2018.



933

934

935

Fig. 9. Modeled annual flash flood casualty cost density difference between the current WSR-88D network and perfect WSR-88D-like coverage.